Vol.3, No.5, Page 1222- 1228, 2025 https://doi.org/10.59628/jast.v3i5.2226 ISSN 2958-9568 JAST

SUN PUBLISHER

مجلة جامعة صنعاء للعلوم التطبيقية والتكنولوجيا

Sana'a University Journal of Applied Sciences and Technology

https://journals.su.edu.ye/index.php/jast/

Optical Forces Induced by a Pulsed LG_{0l} modes on a Nano-Dielectric Spheres

G. A. Alakhaly [1], F. M. Thabit [2] and M. A. Shukri [2*]

[1] **Department of Physics, Faculty Of Education, Humanities and Applied Sciences-Khawlan, Sana'a University, Yemen,**
[2] **Department of Physics, Faculty Of Science, Sana'a University, Sana'a, Yemen.**

*Corresponding author: mshukri@su.edu.ye

Abstract

Theoretically, this study investigates the optical forces induced by a pulsed LG_{0l} modes on nano-dielectric spheres with low and high refractive indices. We analyze how trapping efficiency depends on the particle's refractive index and the beam's azimuthal mode in terms of force magnitude, effective trapping region, and the number of trapping zones. The theoretical model considers dielectric spheres immersed in an oil medium and irradiated by the beam. The results demonstrate that a pulsed LG_{0l} beam achieves higher and more stable trapping efficiency for small azimuthal mode values, short pulse duration, and particles with high refractive indices. Theoretical analysis suggests that the LG_{0l} mode enables 2D trapping of particles with bottle-beam-like control.

Article Info

Keywords:
Laguerre–Gaussian beam, Pulsed Beam, Dipole Approximation, Optical Force, Trapping force, Optical Manipulation.

Article History:
Received: 7-September-2025,
Revised: 23-October-2025,
Accepted: 24-October-2025,
Available online: 28 October 2025.

1. INTRODUCTION

The ability of light to manipulate matter at microscopic and nanoscopic scales has revolutionized optical physics, enabling the development of advanced optical trapping and manipulation techniques that have also impacted biology and nanotechnology [1–15]. Optical tweezers, first demonstrated by Ashkin in 1986, showed that tightly focused laser beams can trap and control microscopic particles with remarkable precision [16]. While conventional Gaussian beams are widely used, they have limited capacity to impart rotational motion or efficiently trap nanoscale objects [7, 17–26].

Recent advances exploit structured light fields [27–30], such as Laguerre–Gaussian (LG_{pl}) beams, which exhibit doughnut-shaped intensity profiles and helical phase fronts carrying orbital angular momentum (OAM) [31–34]. These beams, commonly referred to as vortex beams, can exert both linear forces and rotational torques, thereby enabling controlled rotation, helical transport, and enhanced trapping stability [6, 35–37].

On the other hand, pulsed illumination provides high peak intensities over ultrashort durations, giving rise to transient forces that can exceed steady-state limits and overcome Brownian motion, thereby enabling ultrafast and precise manipulation of nano-dielectric spheres [20, 21, 23–26]. Recent studies have shown that ultrashort pulses can induce transient optical forces that significantly enhance trapping efficiency, rotational control, and particle responsiveness at the nanoscale [38–42].

Several theoretical studies have investigated optical forces within the dipole approximation [20, 21, 26, 40–46]. This study focuses on the LG_{0l} mode, which features two intensity peaks separated by a dark region in two dimensions and is particularly useful for trapping particles or atoms in a planar (2D) configuration. This beam exhibits behavior closely resembling that of a bottle beam, enabling effective control in the two confined dimensions. Furthermore, it can be generated using a significantly simpler setup compared to a full 3D bottle beam [42, 47–49], making it a practical choice for applications such as nanoparticle manipulation or studying atomic transitions in reduced dimensions.

In this study, we investigate the optical forces generated by pulsed LG_{0l} mode on nano-dielectric spheres, with particular focus on how beam topology, pulse duration, and intensity profile govern these forces for two different particle types. We elucidate the mechanisms that enable stable trapping and precise manipulation, offering valuable insights for ultrafast nanophotonic applications, optical assembly, and high-precision particle control. The theoretical framework is presented in Section 2, followed by a discussion of the results in Section 3, and concluding remarks in Section 4.

2. THEORETICAL FORMULATION

A dielectric sphere of radius a and refractive index n_p is immersed in oil with refractive index n_m, and is illuminated by a pulsed Laguerre–Gaussian beam of mode LG_0l as depicted schematically in Fig.1. The polarization of the pulsed electric field is assumed to be along the x-axis. According to Ref. [40], the expression for the electric field of a paraxial pulsed Laguerre–Gaussian beam with radial index $p = 0$ and azimuthal index l is given by:

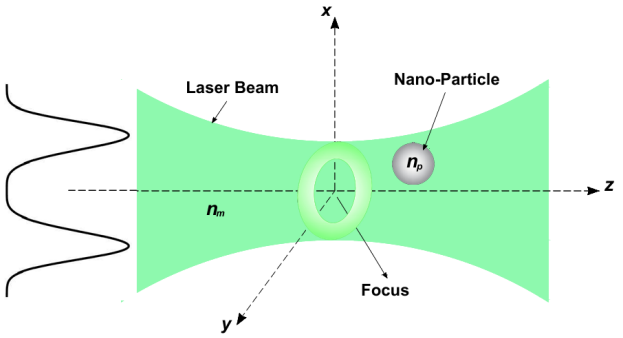

Figure 1. Schematic Diagram for laser beams radiating on a particle.

$$\mathbf{E}_{0l}^{LG}(\rho,\varphi,z,t) = \hat{\mathbf{e}}_\mathbf{x}\, E_0 \,\frac{w_0}{w(z)}\left(\frac{\sqrt{2}\rho}{w(z)}\right)^l L_0^l\left(\frac{2\rho^2}{w(z)^2}\right) \times \exp\left[\left(i\omega_0 t - \frac{\rho^2}{w(z)^2} + ikz - i(l+1)\zeta(z) + ik\frac{\rho^2}{2R(z)} + il\varphi\right)\right] \exp\left(-\frac{(t-z/c)^2}{\tau^2}\right), \tag{1}$$

where $w(z) = w_0\sqrt{1+\frac{z^2}{z_R^2}}$ is the beam width, $R(z) = z\left(1+\frac{z_R^2}{z^2}\right)$ is the wavefront radius, $\zeta(z) = \tan^{-1}\left(\frac{z}{z_R}\right)$ is the phase correction, $z_R = \frac{k w_0^2}{2}$ is the Rayleigh range, w_0 is the Gaussian beam waist at $z = 0$, $L_0^l(.)$ is the associated Laguerre polynomials, E_0 is a constant, $k = \frac{2\pi}{\lambda}$ is the wave number, λ is the wave length, $c = \frac{1}{\sqrt{\epsilon_0\,\mu_0}}$ is the speed of light in vacuum, ϵ_0 and μ_0 are the permittivity and permeability in the vacuum respectively, τ is the pulse duration, $\hat{\mathbf{e}}_\mathbf{x}$ is the unit vector of the polarization along the x direction, ω_0 is the carrier frequency, l determines the phase distribution around the azimuthal direction, ρ is the radial coordinate, φ is the azimuthal coordinate and z is the axial coordinate.

This study examines the optical forces on a subwavelength spheres ($a << \lambda$) by a pulsed Laguerre–Gaussian beam (LG_{0l}), using the dipole approximation.

The pulse intensity is expressed as the time-averaged Poynting vector:

$$\mathbf{I}(\rho,z,t) \equiv \langle \mathbf{S}(\rho,z,t)\rangle_T$$

where

$$\mathbf{S} = \frac{1}{2}\,Re[\mathbf{E}\times\mathbf{H}^*]$$

. Under the paraxial approximation, the magnetic field is approximated by:

$$\mathbf{H} \cong \hat{\mathbf{e}}_\mathbf{y}\, n_m\, \epsilon_0\, c\, E(\rho,z,t)$$

Accordingly, the intensity can be expressed as:

$$\mathbf{I}_{0l}^{LG}(\tilde{\rho},\tilde{z},\tilde{t}) = \hat{\mathbf{e}}_\mathbf{z}\,\frac{2\sqrt{2}\,U}{l!\,\pi^{3/2}\,\tau\,w_0^2\,(1+4\tilde{z}^2)}\left(\frac{2\tilde{\rho}^2}{1+4\tilde{z}^2}\right)^l \times\left[L_0^l\left(\frac{2\tilde{\rho}^2}{1+4\tilde{z}^2}\right)\right]^2 \exp\left[-\frac{2\tilde{\rho}^2}{1+4\tilde{z}^2} - 2\left(\tilde{t}-\frac{\tilde{z}\,k\,w_0^2}{c\,\tau}\right)^2\right], \tag{2}$$

where U is the input energy of the beam and $\hat{\mathbf{e}}_\mathbf{z}$ is a unit vector in the beam propagation direction. In Eq. 2 we have defined the dimensionless parameters for simplicity:

$$\tilde{\rho} = \rho/w_0,\ \tilde{z} = z/kw_0^2,\ \tilde{t} = t/\tau$$

The electric field amplitude is given by:

$$E_0^2 = \frac{4\sqrt{2}\,U}{l!\,n_m\,\epsilon_0\,c\,\pi^{3/2}\,w_0^2\,\tau},$$

The optical force exerted on a dielectric sphere located at position $\mathbf{r}$ is calculated using the Lorentz force, which is the sum of the contributions from the electric $\mathbf{E}$ and the magnetic $\mathbf{B}$ contributions [50]:

$$\mathbf{F}(\mathbf{r},t) = [\mathbf{p}(\mathbf{r},t).\nabla]\,\mathbf{E}(\mathbf{r},t) + \frac{\partial\,\mathbf{p}(\mathbf{r},t)}{\partial\,t}\times\mathbf{B}(\mathbf{r},t), \tag{3}$$

where $\mathbf{p} = \gamma\,\mathbf{E}$ is the dipole moment of the particle, $\gamma = 4\pi\,n_m^2\,\epsilon_0\,a^3\,(m^2-1/m^2+2)$ is the polarizability of a spherical particle in the Rayleigh regime, and $m = n_p/n_m$. After some mathematical relations and identities in Eq. 3, we get

$$\mathbf{F}(\rho,z,t) = \hat{\mathbf{e}}_\mathbf{x}\frac{\gamma}{2}\frac{\partial E_x^2}{\partial\rho} + \hat{\mathbf{e}}_\mathbf{z}\frac{\gamma}{2}\frac{\partial E_x^2}{\partial z} + \hat{\mathbf{e}}_\mathbf{z}\frac{\gamma\,n_m}{c}\frac{\partial E_x^2}{\partial t}, \tag{4}$$

where the first term in Eq. 4 represents the transverse

component of gradient force $(F_{g\rho})$, the second term represents the axial component of gradient force (F_{gz}) and the third term corresponds to F_t, the force arising from the pulse contribution. The components of the pulsed LG force can then be expressed as follows:

$$\mathbf{F}_{g\rho}^{LG}(\tilde{\rho},\tilde{z},\tilde{t}) = -\hat{\mathbf{e}}_{\mathbf{x}}\frac{2\gamma}{n_m\,\epsilon_0\,c\,w_0}\frac{I_{0l}^{LG}(\tilde{\rho},\tilde{z},\tilde{t})}{\tilde{\rho}}\left[\frac{2\tilde{\rho}^2}{1+4\tilde{z}^2}-l\right], \tag{5}$$

$$\mathbf{F}_{gz}^{LG}(\tilde{\rho},\tilde{z},\tilde{t}) = -\hat{\mathbf{e}}_{\mathbf{z}}\frac{4\gamma\,I_{0l}^{LG}(\tilde{\rho},\tilde{z},\tilde{t})}{n_m\,\epsilon_0\,c\,k\,w_0^2}\left[\frac{\tilde{z}\,k^2\,w_0^4}{\tau^2\,c^2}-\frac{\tilde{t}\,k\,w_0^2}{\tau\,c}\right. \\ \left.-\frac{2\tilde{z}}{1+4\tilde{z}^2}\left(\frac{2\tilde{\rho}^2}{1+4\tilde{z}^2}-(l+1)\right)\right], \tag{6}$$

$$\mathbf{F}_{t}^{LG}(\tilde{\rho},\tilde{z},\tilde{t}) = -\hat{\mathbf{e}}_{\mathbf{z}}\frac{8\gamma\,\mu_0\,\tilde{t}}{\tau}I_{0l}^{LG}(\tilde{\rho},\tilde{z},\tilde{t}) \\ +\hat{\mathbf{e}}_{\mathbf{z}}\frac{8\gamma\,\mu_0\,\tilde{z}\,k\,w_0^2}{\tau^2\,c}I_{0l}^{LG}(\tilde{\rho},\tilde{z},\tilde{t}), \tag{7}$$

The scattering force, $\mathbf{F}_{Scat}$, resulting from the scattering of light by the sphere, is proportional to the light intensity and acts along the direction of beam propagation. It can be expressed as [17]:

$$\mathbf{F}_{Scat}^{LG}(\tilde{\rho},\tilde{z},\tilde{t}) = \hat{\mathbf{e}}_{\mathbf{z}}\frac{n_m}{c}\,\alpha\,I_{0l}^{LG}(\tilde{\rho},\tilde{z},\tilde{t}) \tag{8}$$

where $\alpha = \left(\frac{8\pi}{3}\right)(ka)^4\,a^2\left[\frac{m^2-1}{m^2+2}\right]^2$ is the radiation pressure cross section of a spherical particle in the Rayleigh regime.

3. RESULTS AND DISCUSSIONS

Building upon the theoretical framework outlined above, several key results are derived and presented in this section. Unless stated otherwise, all figures have been generated using the parameter set: $\lambda = 0.5145\,\mu m$, $w_0 = 1\,\mu m$, $U = 0.1\,\mu J$, $n_p = (1.33 \text{ and } 2.2)$ (water drop and titanium dioxide nanoparticle), $n_m = 1.7$ (oil) and $a = 5\,nm$.

Figure 2 presents the phase distribution of a Laguerre–Gaussian (LG) beam at $p = 0$ for different values of the topological charge l. The phase map exhibits a helical structure centered on the beam axis, with the number of phase windings increasing proportionally with l. This distinctive phase topology, characteristic of LG beams, influences the spatial distribution of the optical field and, consequently, the optical forces exerted on nanoscale particles. Although LG beams inherently carry an orbital angular momentum (OAM) of $l\hbar$ per photon, which is associated with optical torque, the primary relevance in this study lies in how the helical phase profile modifies the intensity gradients and propagation characteristics that govern optical trapping and manipulation forces.

Figure 3 illustrates the relationship between intensity and transverse and axial distances for different

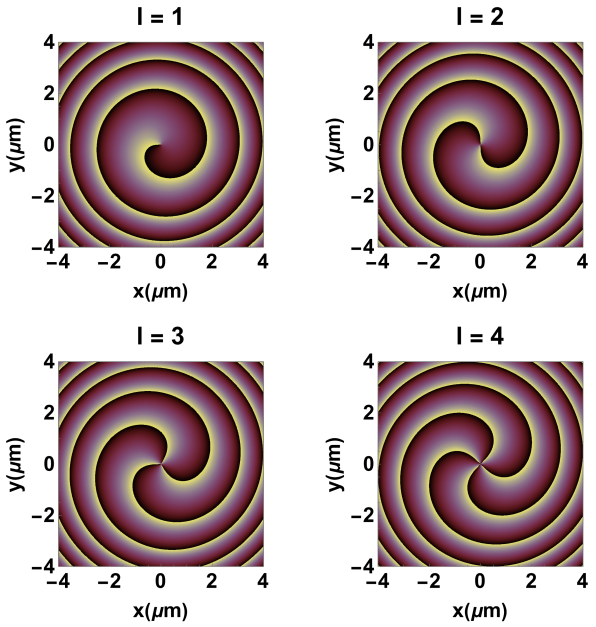

Figure 2. Helical phase structure of a Laguerre–Gaussian (LG) beam $(p = 0)$ illustrating the effect of topological charge l.

values of l and τ at $z = 0$. Sub-figures 3 (a-c) at $\tau = 0.1\,ps$ and sub-figures 3 (d-f) at $\tau = 0.01\,ps$. These sub-figures reveal that, the intensity values decrease with increasing beam mode value l and pulse duration τ. There are only two prominent intensity peaks indicating that two trapping regions are clearly dominant. The inter-peak distance between the two prominent peaks increases as the l-mode value increases. Furthermore, the area of trapping zone shrinks along the z-axis toward $z = 0$. In sub-figures 3 (g,h) it is found that the number of trapping zones changes with varying z-values.

Figure 4 shows the relation between the potential well and the transverse and axial distances for two particles. Sub-figures 4 (a,b) are for high refractive index particle and sub-figures 4 (c,d) are for low refractive index particle. From these sub-figures, it can be seen that the potential well depth decreases with increasing l-mode value, because the beam intensity decreases as l increases, as shown in Fig. 3. Also, the potential well depth of the high refractive index particle is longer than that of the low refractive index one. The well shape changes with varying z values as well.

Figure 5 illustrates the behavior of transverse gradient force against the transverse distance for high and low refractive index particles at different l-mode values. Sub-figures 5 (a,b) are for high refractive index particle, while sub-figures 5 (c,d) are for low refractive index particle. In case of high refractive index particle, two stable trapping zones are existing along the sides of trap center $(\rho = 0)$. While in the case of low refractive index particle, only one stable trapping

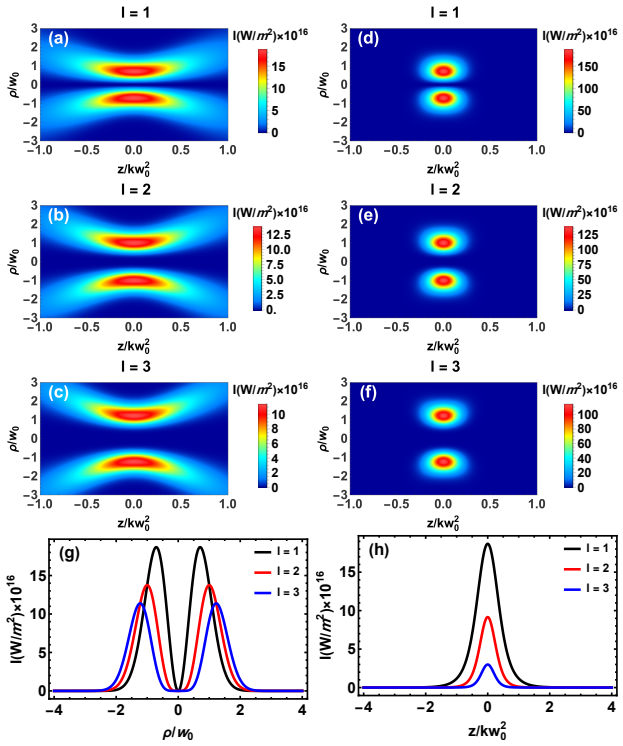

Figure 3. (a-f) Show the intensity distribution of pulsed LG_0l for different values of l and τ at $t = 0$. (a-c) For $\tau = 0.01\,ps$, (d-f) for $\tau = 0.1\,ps$. (g) Shows the intensity profile of pulsed LG_0l for different values of l at $\tau = 0.1\,ps$, $t = 0$ and $z = 0$. (h) Shows the intensity profile of pulsed LG_0l for different values of l at $\tau = 0.1\,ps$, $t = 0$ and $\rho = 0.7\,w_0$.

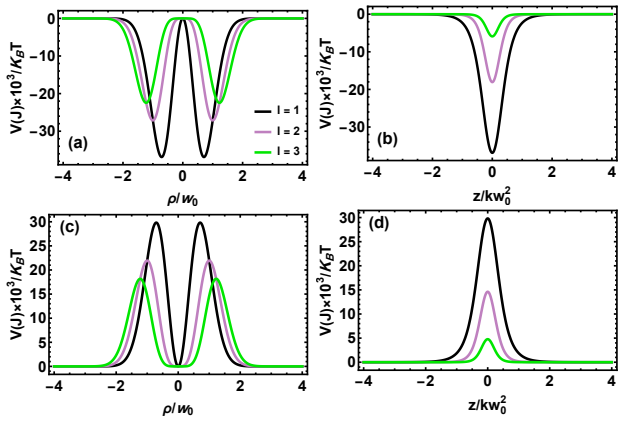

Figure 4. Shows the relation between the potential well and the transverse and axial distances for two particles at $\tau = 0.1\,ps$ and $t = 0$. (a,b) For high refractive index particle at $z = 0$ and $\rho = 0.7\,w_0$ respectively. (c,d) For low refractive index particle at $z = 0$ and $\rho = 0.7\,w_0$ respectively.

zone is presenting at the trap center. In both particles, the transverse gradient force increases with decreasing l-mode value. The central distance between the two forces acting at $\rho = 0$ increases with increasing l-mode value, however, this distance may has a great influence on the trapping performance. This means that at suitable central distance, trapping of more than one particle can be done, but at large central distance the trapping might not be existed depending on force values. The transverse gradient force values are larger in case of high refractive index particle than those of the low refractive index one. In figures 5 and 7, the upward peaks represent the optical force directed to the right, while the downward peaks correspond to the optical force directed to the left.

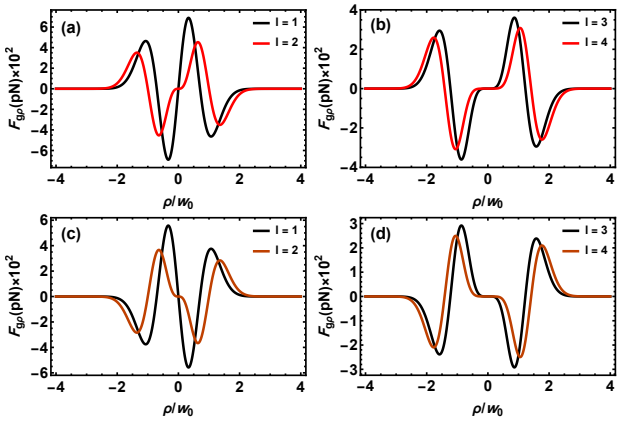

Figure 5. Shows the behavior of the transverse gradient force against the transverse distance for different values of l-mode at $t = 0$, $z = 0$ and $\tau = 0.1\,ps$. (a,b) For high refractive index particle and (c,d) for low refractive index particle.

Figure 6 demonstrates the transverse gradient force distribution for different values of l-mode and pulse duration τ for both low and high refractive index particles. Sub-figures 6 (a-d) are for high refractive index particle, while sub-figure 6 (e-h) are for low refractive index particle. In this figure, it is found that the trapping force value increases with decreasing pulse duration and l-mode values. The area of trapping zone shrinks because of decreasing of pulse duration. In figures 6 and 8, the orange-yellow regions indicate that the optical force is directed upward and to the right, whereas the blue regions indicate that the force is directed downward and to the left.

Figure 7 illustrates the relation between the axial force and the axial distance at different values of l-mode for both low and high refractive index particles. Sub-figures 7 (a,b) represent the high refractive index particle while sub-figures 7 (c,d) are for low refractive index particle. One stable trapping zone is existing for high refractive index particle while nothing is remarked for low refractive index one. The axial force decreases with increasing l-mode values. However, at large l-mode value, the axial force is remarkably decreased compared with those values revealed at small l-mode values. The axial force of high refractive index particle is larger than that of low refractive index particle.

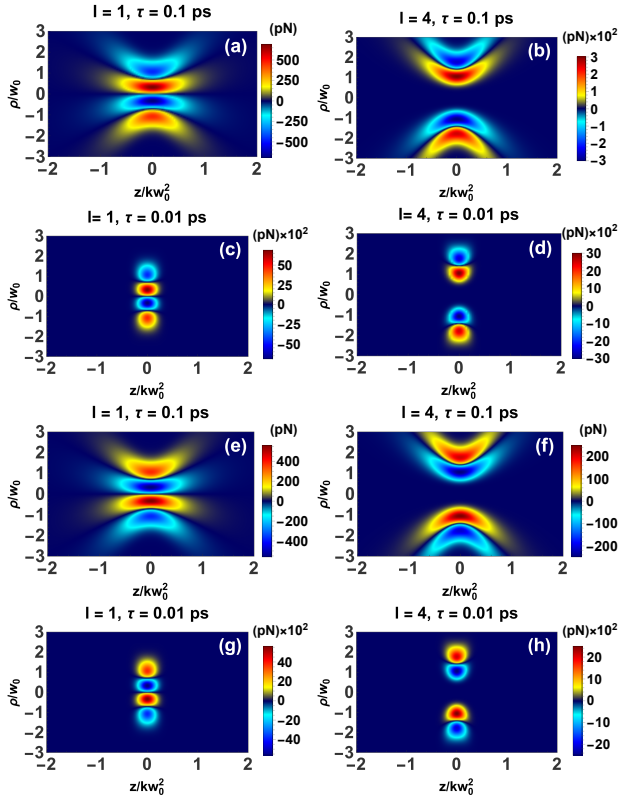

Figure 6. Illustrates the transverse gradient force distribution for different values of l-mode and pulse duration τ at $t = 0$. (a-d) For high refractive index particle and (e-h) for low refractive index particle.

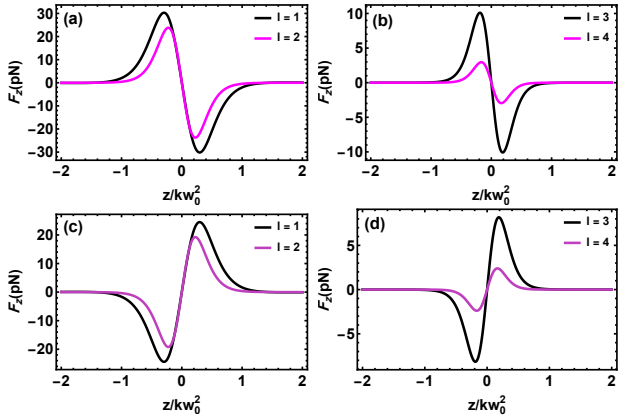

Figure 7. Shows the behavior of the axial force against the axial distance for different values of l-mode at $t = 0$, $\rho = 0.7\, w_0$ and $\tau = 0.1\, ps$. (a,b) For high refractive index particle and (c,d) for low refractive index particle.

Figure 8 presents the axial force distribution for varying values of the l-mode and pulse duration τ for both low- and high-refractive-index particles. Sub-figures 8 (a–d) correspond to high-refractive-index particles, whereas sub-figures 8 (e–h) represent low-refractive-index particles. The results indicate that the axial force increases with decreasing pulse duration and l-mode values. Furthermore, the extent of the trapping region along the z-axis diminishes as the pulse duration decreases. For high-refractive-index particles, two distinct stable trapping zones are observed at larger pulse duration; however, these zones vanish at shorter pulse duration, leaving only the guiding forces dominant. In contrast, for low-refractive-index particles, two stable trapping zones persist for both large and small pulse duration.

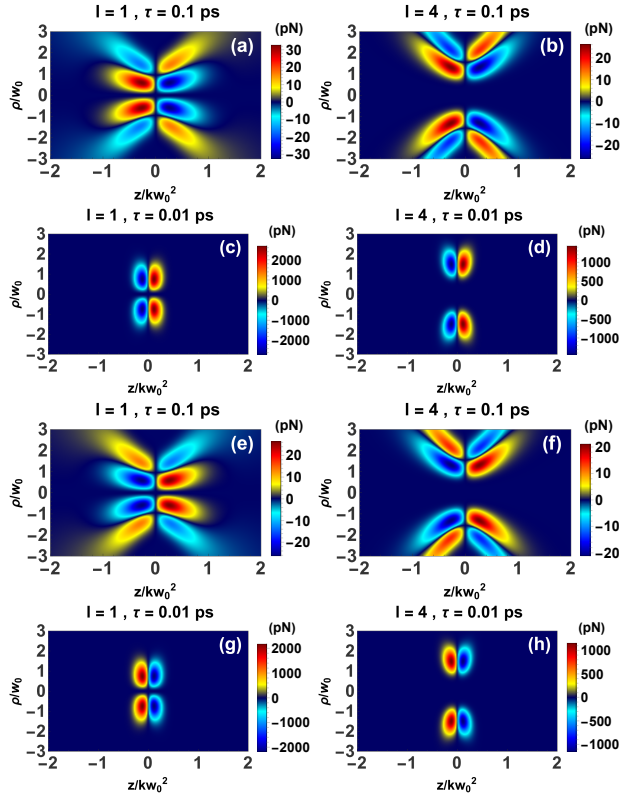

Figure 8. Illustrates the axial force distribution for different values of l-mode and pulse duration τ at $t = 0$. (a-d) For high refractive index particle and (e-h) for low refractive index particle.

4. CONCLUSIONS

Our analysis shows that particles with a high refractive index experience significantly stronger forces compared to those with a low refractive index. The area of force influence depends on the pulse duration but remains unaffected by variations in the azimuthal mode (l). This feature can be advantageous for controlling the number of particles that can be trapped or guided within the same region. Moreover, the number of trapping zones is not influenced by the $l-$mode values or the pulse duration; rather, it is affected by changes in the axial position (z) and the relative refractive index (m), whether $m > 1$ or $m < 1$. Theoretical analysis indicates that the LG_{0l} mode can trap particles or atoms in a planar (2D) configuration, offering bottle-beam-like control in the confined dimensions. These findings provide valuable insights for advancing optical manipulation techniques, with potential

applications in biophotonics, nanotechnology, and the controlled assembly of micro- and nano-scale systems.

REFERENCES

[1] A. Ashkin and J. M. Dziedzic, "Optical trapping and manipulation of viruses and bacteria," *Science*, vol. 235, no. 4795, pp. 1517–1520, 1987.

[2] K. Dholakia, M. P. MacDonald, P. Zemánek, and T. imr, "Cellular and colloidal separation using optical forces," *Methods Cell Biol.*, vol. 82, pp. 467–495, 2007.

[3] T. A. Nieminen, G. Knoner, N. R. Heckenberg, and H. Rubinsztein-Dunlop, "Physics of optical tweezers," in *Methods in Cell Biology*, vol. 82, 2007, pp. 207–236.

[4] M. J. Padgett, J. Molloy, and D. McGloin, *Optical Tweezers: Methods and Applications*. CRC Press, 2010.

[5] S. Kumar and M. J. Deen, *Fiber optic communications: fundamentals and applications*. John Wiley & Sons, 2014.

[6] D. S. Bradshaw and D. L. Andrews, "Manipulating particles with light: Radiation and gradient forces," *Eur. J. Phys.*, vol. 38, no. 3, p. 034 008, 2017.

[7] Z. Gong, Y.-L. Pan, G. Videen, and C. Wang, "Optical trapping and manipulation of single particles in air: Principles, technical details, and applications," *J. Quant. Spectrosc. Radiat. Transf.*, vol. 214, pp. 94–119, 2018.

[8] C.-Y. Chuang, M. Zammit, M. L. Whitmore, and M. J. Comstock, "Combined high-resolution optical tweezers and multicolor single-molecule fluorescence with an automated single-molecule assembly line," *The J. Phys. Chem. A*, vol. 123, no. 44, pp. 9612–9620, 2019.

[9] H. Xin, Y. Li, Y.-C. Liu, Y. Zhang, Y.-F. Xiao, and B. Li, "Optical forces: From fundamental to biological applications," *Adv. Mater.*, vol. 32, no. 37, p. 2 001 994, 2020.

[10] C. A. Campugan, K. R. Dunning, and K. Dholakia, "Optical manipulation: A step change for biomedical science," *Contemp. Phys.*, vol. 61, no. 4, pp. 277–294, 2020.

[11] H. L. et al., "Optical pulling forces and their applications," *Adv. Opt. Photonics*, vol. 12, no. 2, pp. 288–366, 2020.

[12] J. M. et al., "Optomechanics with levitated particles," *Rep. Prog. Phys.*, vol. 83, no. 2, p. 026 401, 2020.

[13] G. Pesce, P. H. Jones, O. M. Maragò, and G. Volpe, "Optical tweezers: Theory and practice," *Eur. Phys. J. Plus*, vol. 135, pp. 1–38, 2020.

[14] I. A. Favre-Bulle and E. K. Scott, "Optical tweezers across scales in cell biology," *Trends Cell Biol.*, vol. 32, no. 11, pp. 932–946, 2022.

[15] H. Hwang, A. Byun, J. Park, S. de Léséleuc, and J.-w. Ahn, "Optical tweezers throw and catch single atoms," *Optica*, vol. 10, no. 3, pp. 401–406, 2023.

[16] A. Ashkin, J. M. Dziedzic, J. E. Bjorkholm, and S. Chu, "Observation of a single-beam gradient force optical trap for dielectric particles," *Opt. letters*, vol. 11, no. 5, pp. 288–290, 1986.

[17] Y. Harada and T. Asakura, "Radiation forces on a dielectric sphere in the rayleigh scattering regime," *Opt. Commun.*, vol. 124, no. 4-5, pp. 529–541, 1996.

[18] A. Ashkin, "Optical trapping and manipulation of neutral particles using lasers," *Opt. Lett.*, vol. 24, no. 5, pp. 54–56, 1999.

[19] A. Ashkin, "History of optical trapping and manipulation of small neutral particles, atoms, and molecules," *Single Mol. Spectrosc.*, pp. 1–31, 2001.

[20] L.-G. Wang and C.-L. Zhao, "Dynamic radiation force of a pulsed gaussian beam acting on a rayleigh dielectric sphere," *Opt. Express*, vol. 15, no. 17, pp. 10 615–10 621, 2007.

[21] L.-G. Wang and H.-S. Chai, "Revisit on dynamic radiation forces induced by pulsed gaussian beams," *Opt. Express*, vol. 19, no. 15, pp. 14 389–14 402, 2011.

[22] J. C. Shane, M. Mazilu, W. M. Lee, and K. Dholakia, "Effect of pulse temporal shape on optical trapping and impulse transfer using ultrashort pulsed lasers," *Opt. Express*, vol. 18, no. 7, pp. 7554–7568, 2010.

[23] L. Cerami, E. Mazur, S. Nolte, and C. B. Schaffer, "Femtosecond laser micromachining," in *Ultrafast Nonlinear Optics*, 2013, pp. 287–321.

[24] N. du Preez-Wilkinson, A. B. Stilgoe, T. Alzaidi, H. Rubinsztein-Dunlop, and T. A. Nieminen, "Forces due to pulsed beams in optical tweezers: Linear effects," *Opt. Express*, vol. 23, no. 6, pp. 7190–7208, 2015.

[25] T.-H. Liu, W.-Y. Chiang, A. Usman, and H. Masuhara, "Optical trapping dynamics of a single polystyrene sphere: Continuous wave versus femtosecond lasers," *The J. Phys. Chem. C*, vol. 120, no. 4, pp. 2392–2399, 2016.

[26] M. Shukri and F. Thabit, "Impact of gaussian beam spot size on trapping forces: Continuous versus pulsed beams," *Sana'a Univ. J. Appl. Sci. Technol.*, vol. 2, pp. 327–332, 2024.

[27] M. Woerdemann, *Structured light fields: applications in optical trapping, manipulation, and organisation*. Springer Science & Business Media, 2012.

[28] M. Woerdemann, C. Alpmann, M. Esseling, and C. Denz, "Advanced optical trapping by complex beam shaping," *Laser & Photonics Rev.*, vol. 7, no. 6, pp. 839–854, 2013. [Online]. Available: https://doi.org/10.1002/lpor.201200058.

[29] E. Otte and C. Denz, "Optical trapping gets structure: Structured light for advanced optical manipulation," *Appl. Phys. Rev.*, vol. 7, no. 4, p. 041 308, 2020.

[30] Y. Yang, Y.-X. Ren, M. Chen, Y. Arita, and C. Rosales-Guzmán, "Optical trapping with structured light: A review," *Adv. Photonics*, vol. 3, no. 3, pp. 034 001–034 001, 2021.

[31] L. Allen, M. W. Beijersbergen, R. Spreeuw, and J. Woerdman, "Orbital angular momentum of light and the transformation of laguerre-gaussian laser modes," *Phys. review A*, vol. 45, no. 11, p. 8185, 1992.

[32] T. Kuga, Y. Torii, N. Shiokawa, T. Hirano, Y. Shimizu, and H. Sasada, "Novel optical trap of atoms with a doughnut beam," *Phys. Rev. Lett.*, vol. 78, no. 25, p. 4713, 1997.

[33] A. Ohta and Y. Kawata, "Analyses of radiation force and torque on a spherical particle near a substrate illuminated by a focused laguerre–gaussian beam," *Opt. communications*, vol. 274, no. 2, pp. 269–273, 2007.

[34] L.-M. Zhou, K.-W. Xiao, J. Chen, and N. Zhao, "Optical levitation of nanodiamonds by doughnut beams in vacuum," *Laser & Photonics Rev.*, vol. 11, no. 2, p. 1 600 284, 2017.

[35] P. Prentice et al., "Manipulation and filtration of low index particles with holographic laguerre-gaussian optical trap arrays," *Opt. Express*, vol. 12, no. 4, pp. 593–600, 2004.

[36] T. Qu, Z.-S. Wu, Q.-C. Shang, Z.-J. Li, L. Bai, and L. Gong, "Analysis of the radiation force of a laguerre gaussian vortex beam exerted on an uniaxial anisotropic sphere," *J. Quant. Spectrosc. Radiat. Transf.*, vol. 162, pp. 103–113, 2015.

[37] B. Gao, J. Wen, G. Zhu, L. Ye, and L.-G. Wang, "Precise measurement of trapping and manipulation properties of focused fractional vortex beams," *Nanoscale*, vol. 14, no. 8, pp. 3123–3130, 2022.

[38] Y. Jiang, T. Narushima, and H. Okamoto, "Nonlinear optical effects in trapping nanoparticles with femtosecond pulses," *Nat. Phys.*, vol. 6, no. 12, pp. 1005–1009, 2010.

[39] L. Gong, B. Gu, G. Rui, Y. Cui, Z. Zhu, and Q. Zhan, "Optical forces of focused femtosecond laser pulses on nonlinear optical rayleigh particles," *Photonics Res.*, vol. 6, no. 2, pp. 138–143, 2018.

[40] M. Shukri and F. Thabit, "Calculation of the optical forces exerted on a nano-dielectric sphere induced by a pulsed laguerre–gaussian beam," *JOSA A*, vol. 40, no. 4, pp. 645–651, 2023.

[41] M. A. Shukri and F. M. Thabit, "Optical trapping forces exerted by a pulsed hermite–gaussian beam on a dielectric nanosphere," *Results Phys.*, vol. 66, p. 108 020, 2024.

[42] F. Thabit and M. Shukri, "Optical trapping of high and low refractive index nanoparticles using pulsed bottle beam," *Phys. Scripta*, vol. 100, no. 3, p. 035 530, 2025.

[43] H.-S. Chai and L.-G. Wang, "Improvement of optical trapping effect by using the focused high-order laguerre–gaussian beams," *Micron*, vol. 43, no. 8, pp. 887–892, 2012.

[44] J. Su, N. Li, J. Mou, Y. Liu, X. Chen, and H. Hu, "Simultaneous trapping of two types of particles with focused elegant third-order hermite–gaussian beams," *Micromachines*, vol. 12, no. 7, p. 769, 2021.

[45] M. Shukri and F. Thabit, "Calculation of trapping optical forces induced by a focused continuous hermite gaussian beam on a nano-dielectric spherical particle," *Phys. Scripta*, vol. 99, no. 6, p. 065 504, 2024.

[46] F. Thabit and M. Shukri, "Trapping of low and high refractive index nano-spherical particles by using a highly focused laguerre–gaussian beam," *Appl. Opt.*, vol. 63, no. 10, pp. 2614–2620, 2024.

[47] L. Isenhower, W. Williams, A. Dally, and M. Saffman, "Atom trapping in an interferometrically generated bottle beam trap," *Opt. letters*, vol. 34, no. 8, pp. 1159–1161, 2009.

[48] B. Melo, I. Brandão, B. S. Pinheiro da, R. Rodrigues, A. Khoury, and T. Guerreiro, "Optical trapping in a dark focus," *Phys. Rev. Appl.*, vol. 14, no. 3, p. 034 069, 2020.

[49] H. Khalili Avval, M. R. Rashidian Vaziri, and H. Rastegar Moghaddam, "Spinning multiplexed laguerre–gaussian beams," *Opt. Quantum Electron.*, vol. 57, no. 3, p. 189, 2025.

[50] P. Jones, O. Maragó, and G. Volpe, *Optical tweezers*. Cambridge University Press Cambridge, 2015.